


Microstructural modeling of a TiNi beam bending

A.E. Volkov  , M.E. Evard, N.A. Volkova, E.A. Vukolov

Saint Petersburg State University, Saint-Petersburg, Russia

 a.volkov@spbu.ru

Abstract. This work presents a numerical simulation of a TiNi shape memory alloy (SMA) beam deformation in the mode of pure bending. The beam is loaded by a bending moment and experiences temperature variations. The boundary-value problem includes the equations of the mechanical equilibrium and the constitutive relations of the SMA realized by a microstructural model, which accounts for the strains due to elasticity, thermal expansion, and phase transformation. Bending at different temperatures and the shape recovery on heating are simulated. Thickness distributions of the stress and dependences of the deflection on the bending moment and temperature are obtained. Since the microstructural model automatically accounts for the tension-compression asymmetry of TiNi its use for the description of the SMA behavior predicts that the neutral line of the bent beam does not pass through its center.

Keywords: shape memory alloys, bending, boundary-value problem, modeling

Acknowledgements. *This work was supported by the Russian Foundation for Basic Research, grant number 18-01-00594.*

Citation: Volkov AE, Evard ME, Volkova NA, Vukolov EA. Microstructural modeling of a TiNi beam bending. *Materials Physics and Mechanics*. 2023;51(2): 177-186. DOI: 10.18149/MPM.2512023_16.

Introduction

In shape memory alloy (SMA) applications requiring large displacements, SMA parts accumulate and recover deformations in bending mode. These are the active parts of actuators [1,2], medical staples [3], endovascular stents [4], etc. Bending deformation mode is characterized by inhomogeneous stress and strain fields, consisting of tensioned and compressed layers. Since many SMA, such as the widely used TiNi-based alloys, exhibit asymmetry in tensile-compressive mechanical properties [5,6], the functional properties of a curved SMA beam cannot be the same as those of a bar exposed only to tension or only to compression. To find the dependences of the curvature and deflection of the beam under the action of the bending moment, as well as the distribution of the martensite volume fraction and stresses over the cross-section of the beam, it is necessary to solve the boundary value problem.

Boundary value problems for SMA parts present a difficult task because of the peculiarities of SMA mechanical properties, which hamper calculating the evolution of stress and strain fields. A definite success was achieved in solving isothermal problems for SMA in the pseudoelastic or pseudoplastic state: a macroscopic model for SMA [7] was implemented into a finite element computer package ANSYS [8]. In a recent work [9] the authors using a macro model based on the approach of D.C. Lagoudas [10] solved a challenging 2D boundary value problem concerning the calculation of the stress and strain fields near a crack tip. Introducing into the model a fatigue degradation function they succeeded in the prediction of

the cyclic life of a medical stent. The boundary conditions, including non-isothermal loading, are more complicated, and there are examples of solutions only for the simplest one-dimensional problems, such as torsion of a cylinder with the fixed inner surface and a turned outer surface [11], mandrelling and assembling of a thermomechanical pipe coupling [12], the tension of a cylinder loaded with axial force and cooled from the surface [13-15]. In works [12-15] a microstructural model was used, which allowed obtaining a more physically grounded description of SMA behavior but demanding more computer memory for storage of the internal variables and more computation time. In the work [16] a problem of pure bending of a TiNi beam in the isothermal conditions in the austenitic pseudoelastic and martensitic pseudoplastic state was considered. The present work complements these results by the simulation of the shape recovery on heating.

Constitutive relations: microstructural model

Microstructural models have significant advantages since they directly account for the structure of the SMA and the specific features of different mechanisms of deformation. Some of the first such models were reported in the works [17-19]. In the works [18,19] the primary martensite orientation variants are considered to be the plates characterized by the habit plane and the shift direction. The interaction energy between the plates is calculated with the help of J. Eshelby's theory. It is also assumed that these variants are subdivided into several self-accommodating groups in which variants can grow together. It was shown that these models can simulate pseudoelasticity and the shape memory effect. Further development of E. Patoor, A. Eberhardt, and M. Berveiller model [18] was made in [20], in which the interaction matrix for martensite variants in NiTi SMA was derived. This matrix accounted for all self-accommodating groups observed in this alloy. Works [21,22] were probably the first, in which an idea of connecting the thermodynamic principles with the apparatus of statistical physics was suggested. This allowed deriving relevant properties of SMA in analogy to the formalism used for paramagnetic-ferromagnetic systems. In [23] the Boltzmann-type statistical approach was compared with a crystal plasticity model. In both cases, a previously developed self-consistent scheme of the transition from the stress-strain state on the local scale to the global one was used.

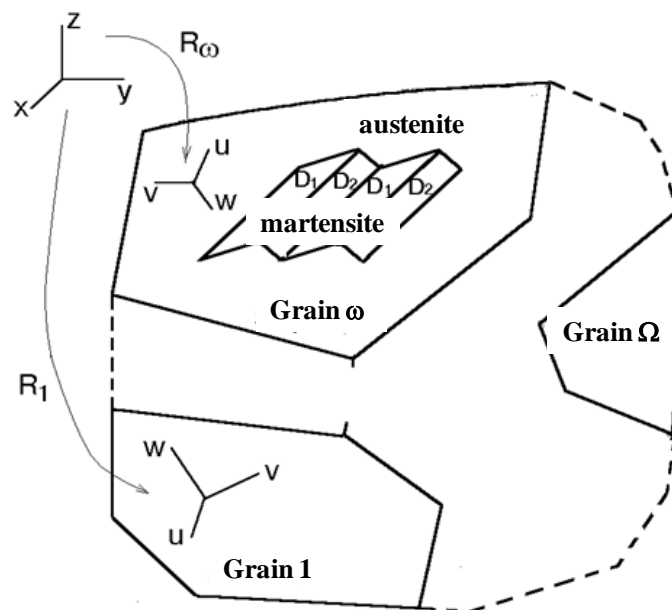


Fig. 1. Scheme of the representative volume of SMA

The microstructural model, which served as the basis for this work, was described in the work [17] and further elaborated in [24-26]. The primary orientational variants of martensite are domains referred to as the Bain's variants, which originate from austenite by one of the variants of the lattice transformation. It was shown that this microstructural model also allowed simulating all the basic phenomena related to the functional-mechanical properties of SMA. The equations are formulated for the phenomena, producing micro-strains of the micro-regions and the macroscopic strain of a representative volume is calculated by neutralization of all micro strains. The internal variables in this model are the volume fractions of Bain's variants. The representative volume V of SMA (Fig. 1) consists of a set of grains, each characterized by the orientation ω of its crystallographic axes.

A. Reuss' hypothesis is accepted and the spatial averaging of the micro-strains is substituted by the orientation averaging. Small deformation tensors are used and the macroscopic strain ε and the volume fraction Φ^M of martensite are:

$$\varepsilon = \sum_{\omega} f(\omega) \varepsilon^{\text{gr}}(\omega), \quad \Phi_M = \sum_{\omega} f(\omega) \Phi^{\text{gr}}(\omega), \quad (1)$$

where the sum is taken over all grains, $f(\omega)$ is the volume fraction of the grains with orientation ω (a discrete analogue of the orientation distribution function) $\varepsilon^{\text{gr}}(\omega)$ and $\Phi^{\text{gr}}(\omega)$ are the strain tensor and the volume fraction of martensite in grain with orientation ω .

In each grain, we consider N variants of martensite obtained from austenite by crystallographically equivalent Bain's deformations D_n ($n = 1, \dots, N$). For TiNi SMA with the transformation of the cubic phase into monoclinic $N=12$. An account of shuffles would increase this number up to 24, but the shuffles do not affect the homogeneous part of the Bain's strain. Thus, we characterize martensite by the internal variables Φ_n ($n = 1, \dots, N$), such that $(1/N)\Phi_n$ is the volume fraction of the domain occupied by the n -th variant of martensite. For the phase deformation of this grain one has:

$$\varepsilon^{\text{gr}} = (1 - \Phi^{\text{gr}}) \varepsilon^A + \frac{1}{N} \sum_{n=1}^N \Phi_n \varepsilon_n^M. \quad (2)$$

The superscripts A and M stand for austenite and martensite, ε^A and ε^M are the deformations of the austenitic and martensitic phases. In this work, we do not take into account plastic and micro-plastic deformations, thus, each of the strains ε^A and ε^M is calculated as the sum of the elastic strain ε^e , thermal expansion strain ε^T , and the phase strain ε^{Ph} . Elastic and thermal strains are assumed to be isotropic and are calculated by common formulae. Since the phase strain is the result of the transformation of austenite to martensite we put that for the austenite $\varepsilon^{\text{PhA}} = 0$ and for the n -th variant of martensite $\varepsilon_n^{\text{PhM}} = D_n$. Then the total phase strain of grain is

$$\varepsilon^{\text{Ph gr}} = \frac{1}{N} \sum_{n=1}^N \Phi_n D_n. \quad (3)$$

The Gibbs' potential G for a unit volume can be written as:

$$G = G^{\text{eig}} + G^{\text{mix}}, \quad G^{\text{eig}} = (1 - \Phi^{\text{gr}}) G^A + \frac{1}{N} \sum_{n=1}^N \Phi_n G_n^M, \quad G_n^{\text{mix}} = \frac{\mu}{2} \sum_{m,n=1}^N A_{mn} \Phi_m \Phi_n, \quad (4)$$

where G^A , G_n^M are the eigenpotentials of austenite and martensite (without an account of their interaction), G^{eig} is the mean value of G^A and G_n^M ; G^{mix} is the "mixing" potential equal to the elastic energy of the interphase stresses, μ is a material constant. In [27] this potential is referred to as the "phase interaction energy function" (PIEF). The eigenpotentials G^A and G_n^M at temperature T and stress σ can be expressed by the formula:

$$G^a = G_0^a - S_0^a(T - T_0) - \frac{c_\sigma^a(T - T_0)^2}{2T_0} - \varepsilon^{0a}(T) : \sigma - \frac{1}{2} \sigma : Q^a : \sigma, \quad a = A, M, \quad (5)$$

where T_0 is the temperature of the thermodynamic equilibrium of austenite and martensite at zero stress, for which the approximation $T_0 = (M_s + A_f)/2$ suggested in [28] is used; G_0^a and S_0^a are the values of the Gibbs' potential and of the entropy at $T = T_0$ and $\sigma = \sigma_0 = 0$; c_σ^a is the specific heat (per unit volume), $\varepsilon^{0a}(T)$ is the strain at $\sigma = \sigma_0$, Q^a is the tensor of elastic compliances, symbol ":" denotes the double scalar product of tensors.

Potential G^{mix} is estimated by a quadratic form of the internal variables Φ_n . Its matrix A_{mn} accounts for the interaction between the Bain's variants of martensite, which in TiNi group into the "Corresponding Variants Pairs" (CVP) [29-31]. This tendency is taken into account by the proposed structure of matrix A_{mn} , which for a proper numeration of variants is:

$$A = \begin{pmatrix} A_1 & 0 & 0 \\ 0 & A_1 & 0 \\ 0 & 0 & A_1 \end{pmatrix}, \quad A_1 = \begin{pmatrix} 1 & -\alpha & -\alpha & 0 \\ -\alpha & 1 & 0 & -\alpha \\ -\alpha & 0 & 1 & -\alpha \\ 0 & -\alpha & -\alpha & 1 \end{pmatrix}, \quad (6)$$

where α is a material constant ($0 \leq \alpha < 1/2$) measuring the degree of the interaction between the variants forming a CVP. The evolution equation for the internal variables is deduced from the condition of equilibrium of the thermodynamic forces F_n , which are the derivatives of the Gibbs' potential.

$$F_n = -\frac{\partial G}{\partial \Phi_n} \approx \frac{q_0(T - T_0)}{T_0} + \sigma : D_n - \mu \sum_{m=1}^N A_{nm} \Phi_m. \quad (7)$$

Here q_0 is the latent heat of the transformation ($q_0 < 0$). The transformation occurs at a state apart from equilibrium when there is an excess of the driving force, i.e at the condition: $F_n = \pm F^{fr}$, with sign "+" taken for the direct and "-" for the reverse transformation. The material constant F^{fr} determines the extent of the deviation from equilibrium and it is responsible for the temperature – phase hysteresis of the transformation.

To describe the reorientation (twinning) of martensite three hypotheses are accepted: (1) any variant of martensite can be transformed in any other variant; (2) reorientation occurs along the direction in the space Φ_1, \dots, Φ_N , corresponding to the fastest decrease of the Gibbs' potential; (3) reorientation starts when the thermodynamic force reaches a critical value. To

find the direction of the reorientation we use vector $F_n = \left\{ -\frac{\partial G}{\partial \Phi_1}, \dots, -\frac{\partial G}{\partial \Phi_N} \right\}$ and take its

projection L onto the plane $\Phi_1 + \dots + \Phi_N = \text{const}$. Then, if for some n it holds that $\Phi_n = 0$ and $L_n < 0$, we substitute L for its projection L' onto the intersection of planes $\Phi_n = 0$ and $\Phi_1 + \dots + \Phi_N = \text{const}$, repeating this procedure for other components of L_n if necessary. Finally, we obtain the direction l , which does not lead to a violation of conditions $\Phi_1 + \dots + \Phi_N < 1$, $\Phi_n > 0$, $n = 1, \dots, N$. For this direction we postulate the condition of reorientation:

$$F^{\text{tw}}(l) = F^{\text{frtw}}, \quad (8)$$

where $F^{\text{tw}}(l) = -\frac{\partial G}{\partial l} = -\sum_{n=1}^N l_n \frac{\partial G}{\partial \Phi_n} = \sum_{n=1}^N l_n F_n$, F^{frtw} is a material constant, characterizing the

critical driving force for reorientation. From hypotheses 1 and 2, it follows that the increments $d\Phi_n$ are proportional to l_n : $d\Phi_n = l_n d\varphi$, where $d\varphi$ is the proportionality factor, which must be found from the condition of reorientation.

There are rather few material constants in the model, in which the elastic thermal and phase deformation are taken into account. The values for most of the constants are found from independent experiments: the Bain's strain is determined from the X-ray diffraction data and the scheme of the crystal lattice deformation; values for F^{fr} and μ are derived from the values

of the characteristic temperatures M_f , M_s , A_s , A_f , and the latent heat q_0 (all of them can be measured on the differential scanning calorimeter). The adjustable parameters are $F^{\text{fr tw}}$ and α . The first of them is related to the phase yield limit of martensite and is easily found from the mechanical test. The second affects the value of the reversible phase strain accumulated on the cooling of the specimen under constant stress: with the growth of α the tendency of the Bain's variants to form self-accommodated configurations becomes more pronounced and the macroscopic phase strain decreases. The number of grains N_{gr} is the model parameter, which affects the anisotropy of a simulated SMA. For a single crystal, the material is anisotropic, becoming almost isotropic when N_{gr} exceeds 300. So, this parameter must correlate to the ratio of the grain diameter to the characteristic dimension of the specimen. For TiNi the values of the constants were determined in previous work [26].

This microstructural approach proved to be efficient for simulating the deformation of a specimen in different states (martensitic, two-phase, and austenitic) as well as strain accumulation on cooling and heating under a constant or varying load.

Boundary-value problem for bending of an SMA beam

We consider a beam with a rectangular cross-section with width b and thickness h , loaded by a bending moment M and thus, experiencing pure bending. The bending scheme and beam dimensions are shown in Fig. 2. We assume that loading is made in isothermal conditions, and the cross-section dimensions are such that heat transfer occurs fast enough for the temperature distribution over the cross-section could be considered homogeneous.

For pure bending, the Bernoulli plane-sections hypothesis and the hypothesis of non-compression of layers are valid. In this case, the strain distribution over the height of the beam is specified by the formula

$$\varepsilon_{zz}(y) = \kappa y + \bar{\varepsilon}, \quad (9)$$

where κ is the curvature of the beam central layer and $\bar{\varepsilon}$ is the relative elongation of this layer. The only non-vanishing stress is σ_{zz} . Further, notations ε and σ are used for ε_{zz} and σ_{zz} .

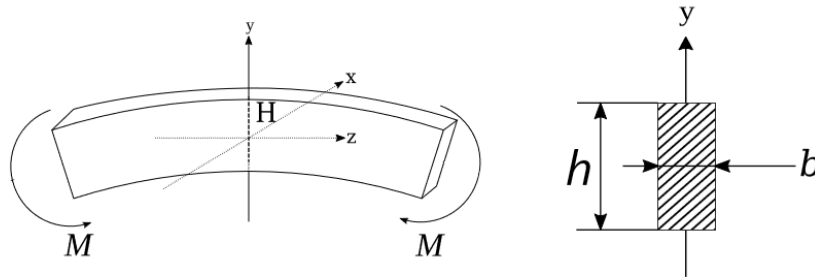


Fig. 2. Scheme of pure bending

The Hook's law gives:

$$\sigma = E(\varepsilon - \varepsilon^{ne}), \quad (10)$$

where E is Young's modulus and ε^{ne} is the non-elastic strain.

For a given distribution $\sigma(z)$ the equilibrium conditions are valid:

$$\int_{-h/2}^{h/2} b\sigma(y)dy = 0, \quad \int_{-h/2}^{h/2} b\sigma(y)ydy = M. \quad (11)$$

The increments of the phase strain and of the internal variables are given by the microstructural model described in section 2. They can be schematically expressed as

$$\Delta\varepsilon^{ne}(y) = F_1(\Delta T, \Delta\sigma(y), X(y)), \quad \Delta X(y) = F_2(\Delta T, \Delta\sigma(y), X(y)), \quad (12)$$

where the functions F_1 and F_2 are defined by the microstructural model and X denotes the set

of internal variables $\Phi_n(\omega)$ – the volume fractions of martensite for each variant n in each grain ω .

To solve the problem specified by equations (9)–(12) we use the discrete scheme, dividing the interval $[-h/2, h/2]$ into K equal segments and search for the values $\sigma_j = \sigma(y_j)$, $\varepsilon_j = \varepsilon(y_j)$, where $y_j = (jh/K)$, $j = 0, \dots, K$.

We split the whole problem into two parts. The first problem is the problem of the mechanical equilibrium and it is to find the "vector" $\{\sigma_j\}$ for given moment M and "vector" $\{\varepsilon_j^{ne}\}$ using formulae (9)–(11). Denoting the operator solving this problem by \mathcal{M} , we write:

$$\{\sigma_j\} = \mathcal{M}(M, \{\varepsilon_j^{ne}\}). \quad (13)$$

The second ("rheological") problem is to find the increments of the non-elastic strains $\{\Delta\varepsilon_j^{ne}\}$ for known increments ΔT and $\{\Delta\sigma_j\}$ using the microstructural model (12). Denoting this operator by \mathcal{R} , we write:

$$\{\Delta\varepsilon_j^{ne}\} = \mathcal{R}(\Delta T, \{\Delta\sigma_j\}). \quad (14)$$

Now we formulate the scheme of passing from the "vector" $\{\varepsilon_j^{ne}(t)\}$ corresponding to the time instant t to the "vector" $\{\varepsilon_j^{ne}(t+\Delta t)\}$, where the time increment Δt corresponds to the increments ΔT and ΔM of the temperature and of the bending moment. This scheme is as follows.

1. Choose the 0-th approximation $\{\varepsilon_j^{ne}\}^{(0)} = 0$ for "vector" $\{\varepsilon_j^{ne}\}$.
2. Find $\{\sigma_j\}^{(1)} = \mathcal{M}(M + \Delta M, \{\varepsilon_j^{ne}\}^{(0)})$.
3. Find the 1-st approximation $\{\varepsilon_j^{ne}\}^{(1)} = \{\varepsilon_j^{ne}\}^{(0)} + \lambda \mathcal{R}(\Delta T, \{\Delta\sigma_j\}^{(1)})$.
4. Repeat steps 1 – 3 until $\max_j(\{\varepsilon_j^{ne}\}^{(i+1)} - \{\varepsilon_j^{ne}\}^{(i)}) < err$,

where λ is the iteration parameter ($0 < \lambda \leq 1$) and err denotes the admissible error.

Thus, for given regime of the thermomechanical loading specified by the successive values of temperature T_i and bending moment M_i corresponding to time instants t_i , one can find the values $\{\varepsilon_j^{ne}(t_i)\}$ and $\{\sigma_j(t_i)\}$ as well as the values κ_i of the curvature.

Simulation results

For simulation the following beam dimensions were chosen: length $l = 50$ mm, width $b = 10$ mm, thickness $h = 2.8$ mm. The characteristic temperatures M_f, M_s, A_s, A_f , were 300, 315, 350, 365 K, and the latent heat $q_0 = -150.0$ J/cm³. The diagram of bending at temperature $T_{def} = 375$ K $> A_f$ is shown in Fig. 3 (the deflection measured at the center of the bent arc) and the height distributions of the stress and phase are presented in Fig. 4.

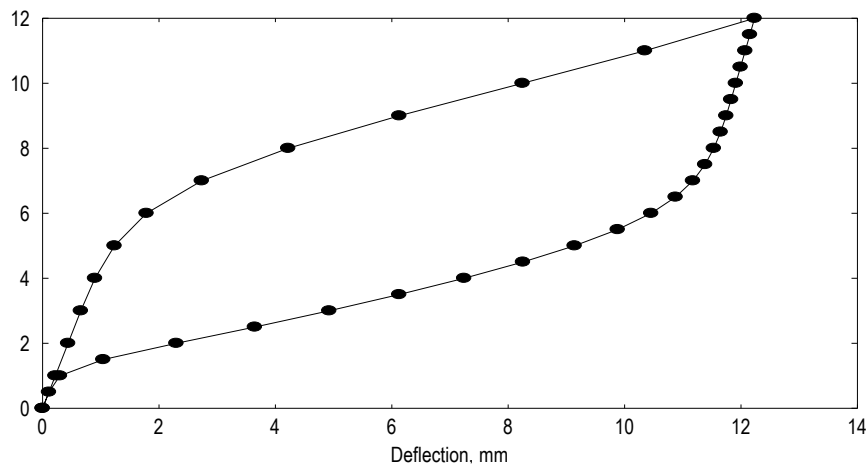


Fig. 3. The dependence of the bending moment on the deflection of the beam for the deformation temperature $T_{def} = 375$ K $> A_f$

The microstructural model automatically accounts for the tension-compression asymmetry of TiNi mechanical properties, the simulation predicts that the neutral line of the bent beam does not pass through its center, but rather is shifted towards the compressed beam layers. In the layers close to the neutral line the total volume fraction of martensite Φ_M is zero, while in both stretched and compressed near-surface layers it has almost the same value ($\Phi_M \approx 0.75$) in spite of the fact that the maximum absolute value of the compressive stress is bigger than of the tensile stress. This circumstance should be taken into account when assessing the functional properties of the SMA tested in bending mode.

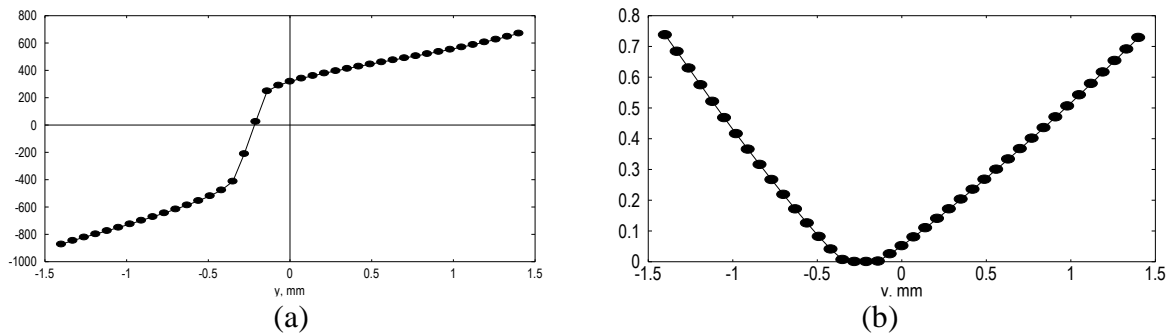


Fig. 4. Distribution of the normal stress (a) and of the volume fraction of martensite (b) along the height of the pseudoelastic beam loaded at 375 K by a bending torque 12 N·m

The next simulation concerned bending of the beam in the pseudoplastic martensitic state, in the two-phase state, and the shape recovery on the subsequent heating. Dependences of the deflection at various temperatures on the bending moment are shown in Fig. 5 and the stress distribution on loading and after unloading are presented in Fig. 6.

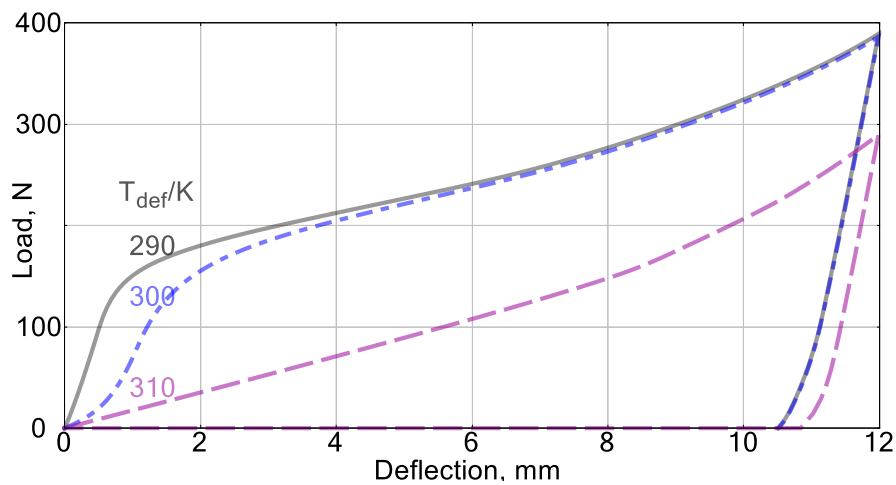


Fig. 5. Dependences of the bending torque on the deflection of the beam during its deformation at temperatures $T_{\text{def}} = 290, 300,$ and 310 K

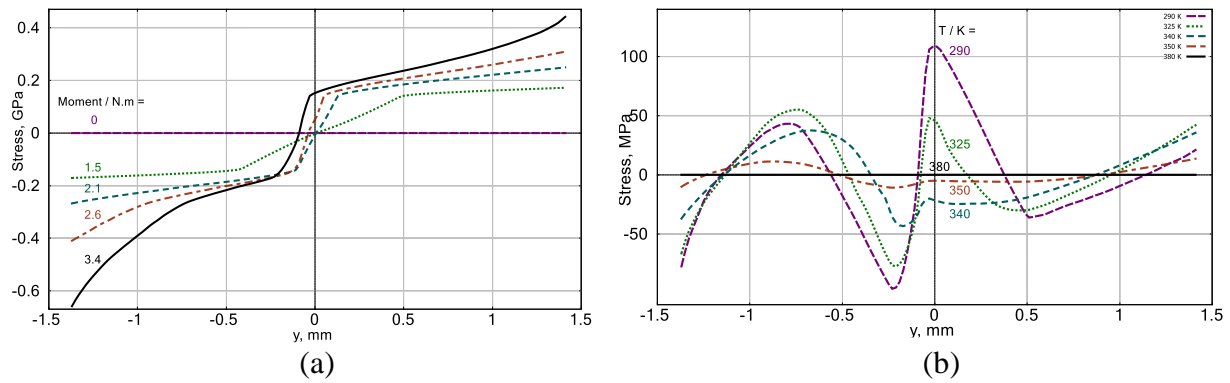


Fig. 6. Distributions of the normal stress along the height of the beam on loading at 290 K (a); after unloading and during consequent heating (b)

Again one can see that the distribution of the stress is not symmetric and the compressive stress is much higher than the tensile one. The asymmetry of the distribution of stress is present also after unloading the beam.

Figure 7 illustrates the shape recovery on heating after the isothermal deformation in the martensitic state and in the thermocycle under a constant bending moment. Because of the internal and applied stresses the reverse transformation temperatures are shifted and the shape recovery starts at a temperature less than A_s .

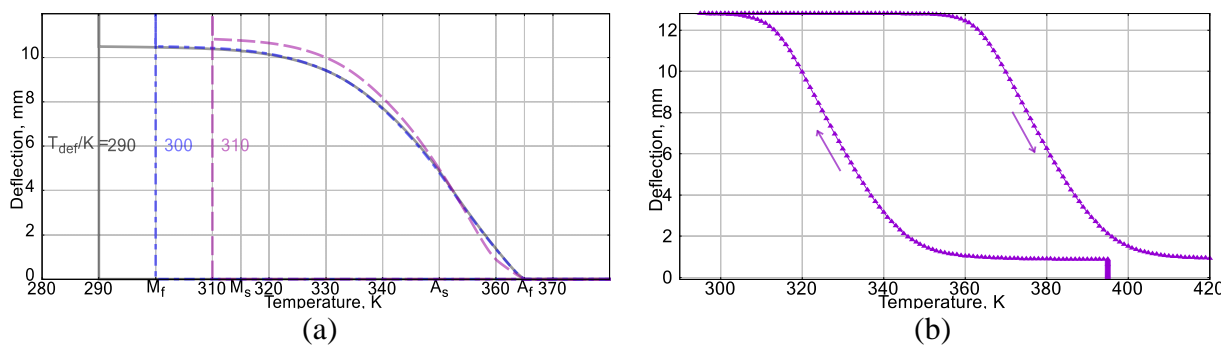


Fig. 7. Dependence of the beam deflection on temperature on heating after isothermal deformation in the martensitic or two-phase state (a); and in the thermocycle under a constant bending moment 4 N·m (b)

Conclusions

1. Microstructural modeling allows solving simple boundary-value problems for thermomechanical loading of SMA in the pure bending mode, revealing the inhomogeneity of the distributions of the stress.
2. The tension-compression asymmetry of SMA leads to the asymmetric distribution of the stress, at which the compressed side of the bent beam is under higher stress than the stretched side.

References

1. Duerig TW, Melton KN, Stöckel D. (Eds.) *Engineering Aspects of Shape Memory Alloys*. Butterworth-Heinemann; 1990.
2. Wanhill RJH, Ashok B. Shape Memory Alloys (SMAs) for Aerospace Applications. In: Prasad N, Wanhill R. (Eds.) *Aerospace Materials and Material Technologies*. Singapore; Springer: 2017.

3. Zhang W, Zhang Y, Zheng G, Zhang R, Wang Y. A Biomechanical Research of Growth Control of Spine by Shape Memory Alloy Staples. *BioMed Research International*. 2013;2013: 384894.
4. Petrini L, Bertini A, Berti F, Pennati G, Migliavacca F. The role of inelastic deformations in the mechanical response of endovascular shape memory alloy devices. *J. of Engineering in Medicine*. 2017;231(5): 391-404.
5. Volkov AE, Emelyanova EV, Evard ME, Volkova NA. An explanation of phase deformation tension–compression asymmetry of TiNi by means of microstructural modeling. *Journal of Alloys and Compounds*. 2013;577(S1): S127-S130.
6. Chatziathanasiou D, Chemisky Y, Meraghni F, Chatzigeorgiou G, Patoor E. Phase Transformation of Anisotropic Shape Memory Alloys: Theory and Validation in Superelasticity. *Shape Memory and Superelasticity*. 2015;1: 359-374.
7. Auricchio F, Petrini L. Improvements and algorithmical considerations on a recent three-dimensional model describing stress-induced solid phase transformations. *Int. J. Numer. Methods*. 2002;55(11): 1255-1284.
8. *Ansys® Academic Research Mechanical APDL*, Release 14.0, Help System, Material Reference/3.24, ANSYS, Inc.
9. Simoes M, Martínez-Pañeda E. Phase field modelling of fracture and fatigue in Shape Memory Alloys. *Computer Methods in Applied Mechanics and Engineering*. 2021;373: 113504.
10. Lagoudas DC. *Shape memory alloys: modeling and engineering applications*. Berlin: Springer; 2008.
11. Rogovoy AA, Stolbova OS. Numerical simulation of the phase transition control in torsion of a hollow cylinder made of heusler alloy. *PNRPU Mechanics Bulletin*. 2019;2019(3): 75-87.
12. Likhachev VA, Razov AI, Volkov AE. Finite difference simulation of a thermomechanical coupling. In: Pelton AR, Hodgson D, Russel SM, Duerig T. (Eds.) *Proceedings of the Second International Conference on Shape Memory and Superelastic Technologies SMST-97, March 2-6, 1997, Asilomar Conference Center, Pacific Grove, California, USA*. 1997. p.335-340.
13. Volkov AE, Kukhareva AS. Calculation of the stress-strain state of a TiNi cylinder subjected to cooling under axial force and unloading. *Bulletin of the Russian Academy of Sciences: Physics*. 2008;72(9): 1267-1270.
14. Volkov AE, Kukhareva AS, Volkova NA, Malkova YV. Size effects in a shape memory alloy rod caused by inhomogeneity of temperature and stress fields studied through solving of a 1d connected thermal and mechanical problem. In: *Proc. of 8th Conference on Smart Structures and Materials, SMART 2017 and 6th International Conference on Smart Materials and Nanotechnology in Engineering, SMN 2017*. 2017. p.1582-1589.
15. Kukhareva A, Kozminskaia O, Volkov A. Calculation of the transformation plasticity strain in the shape memory cylinder. *E3S Web of Conferences*. 2020;157: 06016.
16. Volkov AE, Evard ME, Volkova NA, Vukolov EA. Application of a microstructural model to simulation of a tini beam bending performance and calculation of thickness stress distributions. In: *Proc. of 9th ECCOMAS Thematic Conference on Smart Structures and Materials, SMART*. 2019. p.686-695.
17. Erglis IV, Ermolaev VA, Volkov AE. A model of martensitic unelasticity accounting for the crystal symmetry of the material. *Journal de Physique IV Proceedings, EDP Sciences*. 1995;05(C8): 239-244.
18. Patoor E, Eberhardt A, Berveiller M. Micromechanical modelling of superelasticity in shape memory alloys. *J. de Physique IV*. 1996;06(C1): 277-292.

19. Huang M, Brinson LC. A multivariant model for single crystal shape memory alloy behavior. *J. Mech. Phys. Solids* 1998;46(8): 1379-1409.
20. Niclaeys C, Zineb TB, Patoor E. Influence of Microstructural Parameters on Shape Memory Alloys Behavior. In: Ahzi S, Cherkaoui M, Khaleel MA, Zbib HM, Zikry MA, Lamatina B (eds.) *Proc. of IUTAM Symposium on Multiscale Modeling and Characterization of Elastic-Inelastic Behavior of Engineering Materials*. Dordrecht: Springer; 2004. p.267-274.
21. Fischlschweiger M, Oberaigner ER, Antretter T, Cailletaud G. A multi-block-spin approach for martensitic phase transformation based on statistical physics. *Proc. SPIE 7978, Behavior and Mechanics of Multifunctional Materials and Composites*. 2011;79781H. Available from: <https://doi.org/10.1117/12.881960>.
22. Oberaigner ER, Leindl M. Statistical physics concepts for the explanation of effects observed in martensitic phase transformations. *Smart Materials and Structures*. 2012;21(9): 094020.
23. Fall MD, Patoor E, Hubert O, Lavernhe-Taillard K. Comparative Study of Two Multiscale Thermomechanical Models of Polycrystalline Shape Memory alloys: Application to a Representative volume Element of Titanium–Niobium. *Shap. Mem. Superelasticity*. 2019;5: 163-171.
24. Evard ME, Volkov AE. Modeling of the martensite accommodation effect on mechanical behavior of shape memory alloys. *J. Eng. Mater. and Technol*. 1999;121: 102-104.
25. Volkov AE, Casciati F. Simulation of dislocation and transformation plasticity in shape memory alloy polycrystals. In: Auricchio F, Faravelli L, Magonette G, Torra V. (eds.) *Shape Memory Alloys. Advances in Modelling and Applications*. 2001. p.88-104.
26. Evard ME, Volkov AE, Belyaev FS. A Microstructural Model of SMA with Microplastic Deformation and Defects Accumulation: Application to Thermocyclic Loading. *Materials Today: Proceedings*. 2015;2(3): S583-S587.
27. Nae FA, Matsuzaki Y, Ikeda T. Micromechanical modeling of polycrystalline shape-memory alloys including thermo-mechanical coupling. *Smart Materials and Structures*. 2003;12: 6-17.
28. Salzbrenner RJ, Cohen M. On the thermodynamics of thermoelastic martensitic transformations. *Acta Metallurgica*. 1979;27(5): 739-748.
29. Nishida M, Nishiura T, Kawano H, Imamura T. Self-accommodation of B19' martensite in Ti-Ni shape memory alloys – Part I. Morphological and crystallographic studies of variant selection rule. *Philosophical Magazine*. 2012;92: 2215-2233.
30. Nishida M, Okunishi E, Nishiura T, Kawano H, Imamura T, Ii S, Hara T. Self-accommodation of B19' martensite in Ti-Ni shape memory alloys – Part II. Characteristic interface structures between habit plane variants. *Philosophical Magazine*. 2012;92: 2234-2246.
31. Imamura T, Nishiura T, Kawano H, Hosoda H, Nishida M. Self-accommodation of B19' martensite in Ti-Ni shape memory alloys – Part III. Analysis of habit plane variant clusters by the geometrically nonlinear theory. *Philosophical Magazine*. 2012;92: 2247-2263.